Oxygen-for-Sulfur Exchange in the Gas Phase: Reactions of Al and Si Oxyanions with H_2S

G. S. Groenewold,* B. D. M. Hodges, J. R. Scott, A. K. Gianotto, A. D. Appelhans, and G. F. Kessinger

Idaho National Engineering and Environmental Laboratory, Idaho Falls, Idaho 83415-2208

J. B. Wright

Natick Soldier Center, Natick, Massachusetts 01760-5020

Received: December 14, 2000; In Final Form: February 12, 2001

Gas-phase Si and Al oxyanions were formed by particle bombardment, isolated by mass, and then reacted with H_2S in an ion trap secondary ion mass spectrometer (IT-SIMS). The reactions proceeded by different reaction pathways depending on whether the oxyanions were even- or odd-electron species. The radical anion $SiO_2^{\bullet -}$ reacted with H_2S by abstracting a $^{\bullet}SH$ radical to form the even-electron SiO_2SH^-. Once formed, the even electron SiO_2SH^- reacted with a second H_2S molecule by O-for-S exchange to form $SiOS_2H^-$. The radical anion $SiO_3^{\bullet -}$ abstracted an $^{\bullet}H$ radical from H_2S to form even-electron SiO_3H^-, which then underwent two consecutive O-for-S exchange reactions with H_2S to form SiO_2SH^- and $SiOS_2H^-$. For the reactions of the even-electron anion AlO_2^-, the products of two consecutive O-for-S exchange reactions with H_2S were $AlOS^-$ and AlS_2^-. The radical abstraction reactions and the O-for-S exchange reactions of SiO_3H^-, AlO_2^-, and $AlOS^-$ were efficient in the 30−50% range. The efficiency of the O-for-S exchange reaction of SiO_2SH^- (producing $SiOS_2H^-$) was substantially less efficient at 8%.

I. Introduction

The present research describes the reactions of H_2S with small Si and Al oxyanions, specifically AlO_2^-, $SiO_2^{\bullet -}$, $SiO_3^{\bullet -}$, and SiO_3H^-. Interest in mineral oxyanions stems from the fact that they represent reactive moieties found on geological surfaces. For example, anionic sites found on high-Al clay minerals are known to efficiently bind metal cations that can then initiate surface precipitation reactions.[1−3] A second example is that of terrestrial dust particulates that have anionic surface moieties that may well be important in atmospheric adsorption reactions that affect S, C, and N budgets.[4−7]

The interaction of mineral oxide surfaces with H_2S is a subject of particular interest because (1) H_2S is present in the atmosphere, in catalytic process environments, and in reductive geochemical environments such as uranium acid mine drainage[8] and (2) H_2S binds strongly and influences reactivity properties of mineral oxides. The interactions of H_2S with alumina and aluminosilicates provide good examples of binding behavior. H_2S was found to undergo both H-bonding and alkali metal cation coordination via S when in contact with H- and Na-zeolites, respectively.[9] H_2S has been shown to reduce active sites on a variety of metal oxides, including alumina and alumina-supported Pd and Pt catalysts, forming sulfates in the process.[10−12] This has the effect of poisoning catalytic properties. To better understand H_2S surface modifications, alumina supported Co−Mo hydrodesulfurization catalysts were studied after reaction with H_2S, and it was found that -SH groups were formed on coordinatively unsaturated sites.[13] However, even though much has been learned through these studies of the bulk reactivity of mineral oxyanions with H_2S, the explicit reactivity of oxyanion moieties with H_2S has not been examined in detail.

The reactivity of mineral oxyanions has not been rigorously studied because they are difficult to probe in their native state. Certainly extensive structural information can be gained through the use of synchrotron radiation, X-ray diffraction, Raman spectroscopy, or reflectance infrared spectroscopy techniques. However, the generation of direct reactivity information has been difficult or impossible. The study of mineral oxyanion reactivity in the gas-phase allows the investigation of ion−molecule reactions that enable the intrinsic chemistry of reactive systems to be observed in a manner free from solvent or countercation effects. This approach relies on getting the appropriate reactive moieties into the gas phase. However, mineral oxides have low vapor pressures and are not generated in abundance by sputtering. Consequently, mineral oxides have not been studied extensively in the gas phase.

In our laboratory, an approach has been developed for investigating the reactivity of mineral oxyanions with adsorbate molecules. This approach is based on an ion trap secondary ion mass spectrometer (IT-SIMS). Historically, this instrument has primarily been used for analytical investigations of surface adsorbates such as the nerve agent VX on soil or concrete.[14] However, during these studies it was found that in addition to the adsorbate ions, matrix-derived ions are also sputtered into the gas phase. Initially, ions from aluminum and silicon oxide surfaces that had compositions such as $Al_nO_{2n}H_{n-1}^-$ and $Si_nO_{2n+1}H^-$ were observed, and it was noted that these would undergo gas-phase hydrolysis reactions with background water in the ion trap. This observation led to a systematic investigation of aluminum oxyanion reactivity with H_2O, which showed that AlO_2^- would react inefficiently with one and two H_2O to form $AlO_3H_2^-$ and $AlO_4H_4^-$.[15] In contrast, $Al_2O_4H^-$ reacted with 100% efficiency to add the first H_2O and with ∼50% efficiency to add a second H_2O. More recently, the reactions of silicon oxyanions with H_2O have been investigated. These revealed that the radical $SiO_2^{\bullet -}$ and $SiO_3^{\bullet -}$ would react with H_2O by inefficient radical abstraction and that SiO_3H^- would react by inefficient condensation.[16] In contrast, the condensation of

10.1021/jp004495q CCC: $20.00
Published on Web 03/27/2001

$Si_2O_5H^-$ with H_2O was 50% efficient. These initial H_2O reactivity experiments display some similarities with the H_2S results presented here.

The reactivity investigations were extended to H_2S because H_2S is a stronger acid than is H_2O. We hypothesized that H_2S might participate in proton exchange reactions, providing a means to evaluate the acidity/basicity of the aluminum and silicon oxide species. Furthermore, if fast H/D exchange reactions could be performed, then it would be possible to measure the number of active protons in mixed $Al_mSi_nO_{2(m+n)}H_{(m-1)}^-$ systems generated from zeolite targets.[17] Measurement of the number of active H is important because determination of ion composition is a difficult problem in mixed Al and Si oxide systems, because AlH is isobaric and isovalent with Si. However, neither reversible nor irreversible proton exchange was significant when the Al and Si anions reacted with H_2S. Instead, the Al and Si oxyanions underwent either radical addition or concomitant H_2S addition/H_2O elimination (net O-for-S exchange). The reaction path was found to depend on the radical versus even-electron character of the oxyanions.

II. Experimental Section

Samples. Alumina (Brockman I, neutral, lot no. 09906PQ) was obtained from Aldrich (Milwaukee, WI). Silica (5.24 m^2 g^{-1}, lot no. 0768) was obtained from the QuantaChrome Corporation (Syosset, NY). Powdered samples were attached to the end of a 2.7-mm probe tip with double-sided tape (3M, St. Paul, MN).

Instrumentation. The IT-SIMS instrument utilized in these studies has been described previously.[18−20] Briefly, this IT-SIMS is a modified Finnigan ITMS instrument (Finnigan Corp., San Jose, CA). Modifications include incorporation of a perrhenate (ReO_4^-) primary ion beam gun,[21] an insertion lock for introduction of solid samples, and an offset dynode with multichannel plate detector. The primary ion gun and sample probe tip are collinear and located outside opposite end caps of the ion trap. The primary ion gun was operated at 4.5 keV and produced a ReO_4^- beam with a 1.25-mm diameter at a primary ion current ranging from 300 to 600 pA. A ReO_4^- beam was used because this type of ion beam is more efficient for sputtering intact surface species into the gas phase than atomic particle bombardment.[22,23] The data acquisition and control system uses Teledyne Apogee ITMS Beta Build 18 software that controls routine ITMS functions and a Teledyne HST-1000 filtered noise field (FNF) system (Teledyne Electronic Technologies, Mountain View, CA). Data analysis was performed using SATURN 2000 software (version 1.4, Varian, Walnut Creek, CA).

For ion−molecule reaction experiments, H_2S (99.5%, Matheson Tri-Gas, Montgomeryville, PA) was added via a variable leak valve up to pressures of 1×10^{-6} Torr (as measured on an ion gauge). H_2S was present throughout the ionization/reaction/scanout sequence executed in these experiments (vide infra). Ion gauge pressures were corrected by multiplying the measured gauge pressure by 1.82 according to Bartmess and Georgiadis.[24] D_2S (98% D, Cambridge Isotope Labs, Andover, MA) was added instead of H_2S when performing D-exchange experiments. Concurrent with the addition of H_2S (or D_2S), oxygen was added to a pressure of 1×10^{-6} Torr, which mitigated a deleterious effect that the H_2S had on the emission of ReO_4^- from the primary ion emitter. Control experiments showed that the O_2 would not react with the oxyanions to generate the product ions observed. Helium bath gas was added to reach an operating pressure of 3×10^{-5} Torr (uncorrected). The IT-SIMS base pressure was 3×10^{-8} Torr.

IT-SIMS Parameters. Details of a representative sequence of events for ion−molecule reactions have been previously described.[15] In these experiments, the ion trap was operated with a low mass cutoff of 40 amu. Ionization times were adjusted so that a healthy population of ions was generated. Ionization times ranged from ~50 to 200 ms, during which time the ReO_4^- beam was directed through the ion trap and onto the alumina or silica target. Ion isolation was performed at the same time as ionization (sample bombardment) by applying a notched FNF, where the frequencies of the notch corresponded to the natural frequency of the ion being isolated. This method results in ejection of ions whose natural frequencies do not fall within the notch. Since ion mass is correlated with frequency, mass selective ion isolation is accomplished.

Once the ions were formed and isolated, ion−molecule reactions with H_2S began to occur. The extent of reaction was varied by altering the duration of a delay period between the ionization/isolation event and the ion scan-out/detection event.

After reaction, ions were scanned out of the ion trap using a mass selective instability scan with axial modulation.[25] To account for signal originating from grids on the ion trap end caps, background spectra were collected after each sample was analyzed. Seven spectra (each composed of the average of 15 or 20 scans) were averaged and background corrected to obtain final peak intensities. The relative standard deviation between averaged spectra was ± 5%.

For any given experiment, ion lifetimes (the *x* axis on the kinetic plots) were estimated from the end of the ionization period to the exit of the ions from the trap. The FNF waveform is applied during the ionization period, ejecting all product ions formed during ionization. The delay period made up the majority of the ion lifetime, with corrections included for electronics settle times and time within the scanout period required for ejection of the mass of interest.

To generate kinetic plots, ion abundances were normalized to the sum of the reactant and product ions. The normalization corrected the data for a slow 10−20% apparent increase in ion abundances, which occurred as a result of increased trapping efficiency at longer delay periods. Approximately the same number of ions were generated in experiments that had short or long delay periods; however, at longer delay periods the number of collisions with the He (3×10^{-5} Torr) bath gas was increased. This localized more ions in the center of the trap and improved the efficiency of the scanout and detection. This made the total number of ions in the trap appear to increase over the first 200 ms of the experiment.

Computational Methods. Ab initio molecular orbital calculations were performed for the $AlO_2^- + H_2S$ system using the Gaussian 98 program.[26] All structures were fully optimized using the RB3LYP and UB3LYP exchange and correlation functionals[27,28] with the 6-311+G(2d,2p) basis set. All minimizations were carried out using the Berny algorithm,[29,30] and the default parameters were used for the integral cutoff and minimization convergence criteria. Vibrational frequencies were calculated for all minima.

Calculation of Rate Constants. The reactions of Al and the Si oxyanions with H_2S exhibit pseudo first-order kinetics because the concentration of H_2S is significantly greater than that of the ions produced and therefore remains essentially constant throughout the reaction. The majority of the measurement uncertainty is introduced due to pressure measurement of H_2S. Although the reproducibility of the H_2S pressure measurement is good, the absolute accuracy is somewhat uncertain, especially at low pressures. Replicate experiments using H_2S

and H_2O over a range of pressures gave rate constants that varied by up to 30%, which is probably representative of the uncertainty in the pressure measurement.[15] Therefore, we estimate that the uncertainty in k_1^{exp} is approximately ± 30%.

Reaction efficiency was evaluated by comparing measured rate constants with theoretical rate constants calculated using the average-dipole-orientation (ADO) theory developed by Su and Bowers.[31−33] A temperature of 310 K was used.[33−35]

All of the ions studied underwent consecutive reactions. While the rate constant for the initial reaction, k_1, could be measured directly, the rate constants for the second and third reactions, k_2 and k_3, could only be estimated. The rate constants for the consecutive reactions were estimated using a stochastic kinetic modeling approach that was based on a rigorously derived Monte Carlo procedure that numerically simulates the time evolution of the reactions involved.[36] The stochastic kinetic modeling was performed using the Chemical Kinetic Simulator software package, that is available for a no cost license on the IBM website.[37] The stochastic approach was adopted because it does not require exact solution of coupled differential equations required by the deterministic approach, and hence is much more adaptable to complicated kinetic systems. To validate the stochastic approach, k_2 was also estimated by fitting a deterministic kinetic consecutive reaction model to the reaction profile data for the $SiO_2^{\bullet-} + H_2S$ reaction. The deterministic model was generated using eqs 1−3 for consecutive first-order reactions.[38,39] In these equations, A represents the abundance of the initial reactant ion, B represents the abundance of the intermediate product, and C represents the abundance of the final product at time t. A_0, B_0, and C_0 are the abundances of the ions at $t = 0$.

$$A = A_0 e^{-k_1 t} \tag{1}$$

$$B = B_0 e^{-k_2 t} + \frac{k_1 A_0}{(k_2 - k_1)}(e^{-k_1 t} - e^{-k_2 t}) \tag{2}$$

$$C = C_0 + A_0(1 - e^{-k_1 t}) + B_0\left[1 - e^{-k_2 t} - \frac{A_0/B_0}{1 - k_2/k_1}(e^{-k_2 t} - e^{-k_1 t})\right] \tag{3}$$

III. Results and Discussion

The ions studied for reactivity with H_2S were generated by bombarding silica and alumina particles with energetic projectiles, a process known as SIMS. The negative SIMS spectrum of silica[40] contained low abundance ions corresponding to $SiO_2^{\bullet-}$, $SiO_3^{\bullet-}$, and SiO_3H^-, that could be mass isolated and accumulated using the IT-SIMS (see experimental). These isolated ions were then reacted with H_2S for variable reaction times. Likewise, the negative SIMS spectrum of alumina contained a low abundance AlO_2^- that was mass isolated and reacted with H_2S.[40]

$SiO_2^{\bullet-}$. When $SiO_2^{\bullet-}$ (*m*/*z* 60) was sputtered into the ion trap containing about 1×10^{-6} Torr H_2S, a single reaction product at *m*/*z* 93 appeared after a short time period (Figure 1). This ion corresponded to SiO_2SH^- and must be formed by abstraction of a $^{\bullet}SH$ radical from H_2S by $SiO_2^{\bullet-}$ (reaction 1). The ion

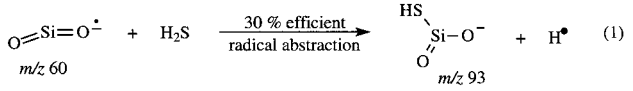

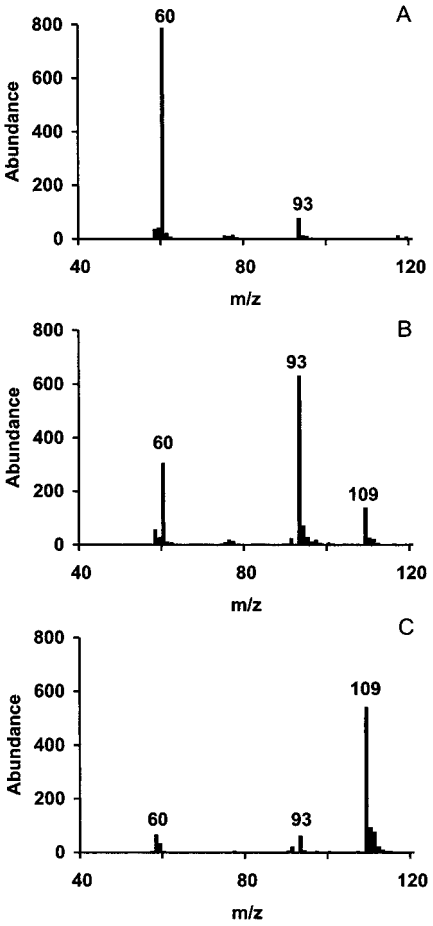

Figure 1. Spectra of isolated $SiO_2^{\bullet-}$ reacting with H_2S at 1.1×10^{-6} Torr. (A) Spectrum after 2 ms. (B) Spectrum after 97 ms. (C) Spectrum after 802 ms. *m*/*z* 60 corresponds to $SiO_2^{\bullet-}$, 93 to SiO_2SH^-, and 109 to $SiOS_2H^-$. Note the S isotopic ions that accompany *m*/*z* 93 and 109.

assignment was supported by the appearance of S isotopic peaks at *m*/*z* 94 and 95, as well as an experiment in which $SiO_2^{\bullet-}$ was reacted with D_2S. In the D_2S experiment, the *m*/*z* 93 ion was shifted to *m*/*z* 94, consistent with the expected composition of SiO_2SD^-.

As the reaction time was increased, a second reaction product appeared at *m*/*z* 109 (reaction 2). The ion composition was

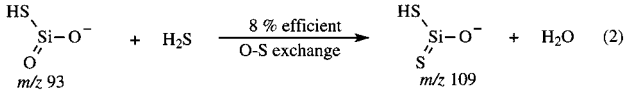

determined to be $SiOS_2H^-$ on the basis of the S isotopic peaks and D-labeling ($SiOS_2D^-$ was formed when D_2S was used). The formation of $SiOS_2H^-$ was unanticipated: it required the formation of an activated adduct ion having the composition $(H_2S{\cdot}SiO_2SH^-)^*$, which must undergo hydrogen rearrangement leading to elimination of H_2O. The reaction of $SiO_2SH^- + H_2S$ (reaction 2) can be described as an O-for-S exchange.

A kinetic plot of the ion abundances versus reaction time clearly showed that the two reactions are sequential (Figure 2), in that the abundance of SiO_2SH^- (*m*/*z* 93) rises and then falls as the final product $SiOS_2H^-$ (*m*/*z* 109) builds in. The semilog plot of the abundance of *m*/*z* 60 versus time was used to calculate a reaction rate constant of 4×10^{-10} cm^3 molecule^{-1} s^{-1}, which is 30% of the theoretical constant calculated using the average dipole orientation (ADO) theory.[31−33] The rate constant for the consecutive reaction $SiO_2SH^- + H_2S \rightarrow$

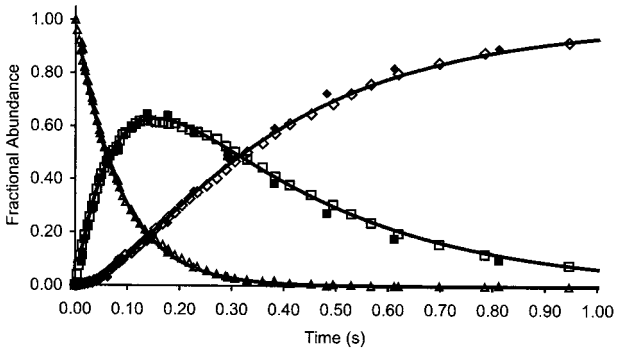

Figure 2. Kinetic plot and modeling of the consecutive reactions $SiO_2^{\bullet-} \rightarrow SiO_2SH^-$, and $SiO_2SH^- \rightarrow SiOS_2H^-$. $P(H_2S) = 1.1 \times 10^{-6}$ Torr. Both deterministic kinetic model and stochastic kinetic model are shown with the experimental data. The $SiO_2^{\bullet-}$ (△), SiO_2SH^- (□), and $SiOS_2H^-$ (◇) represent stochastic models. The deterministic models are represented by lines. Data are represented by $SiO_2^{\bullet-}$ (▲), SiO_2SH^- (■), and $SiOS_2H^-$ (◆).

$SiOS_2H^- + H_2O$ was estimated using two kinetic models: a deterministic consecutive reaction model[38,39] and a stochastic consecutive reaction model.[36,37] Both modeling approaches yielded identical results: the rate constant of the O-for-S exchange reaction of SiO_2SH^- forming $SiOS_2H^-$ was estimated at 0.9×10^{-10} cm^3 molecule^{-1} s^{-1} or about 8% efficient as compared to the ADO constant. Because the stochastic consecutive reaction model was easier to apply to more complex systems, it was selected for modeling the remainder of the ion−molecule reactions in this study.

Once formed, $SiOS_2H^-$ was stable relative to the H_2S environment. The Si displayed no tendency to become tetracoordinate (addition of H_2S), and there was no evidence for an additional O-for-S exchange (which would produce SiS_3H^- at *m*/*z* 125).

The structures of the ions generated in reactions 1 and 2 were investigated using ab initio calculations at the B3LYP/6-311+G(2d,2p) level (Figure 3). The calculations showed that $SiO_2^{\bullet-}$ is a slightly bent molecule, a phenomenon related to the unpaired electron. SiO_2SH^- was calculated to be a tricoordinate structure, with H attached to S. Similarly, $SiOS_2H^-$ was shown to be a tricoordinate structure, with H attached to S. Extensive computational studies are underway to understand the reaction pathway but are proving to be complex due to the radicals involved.

$SiO_3^{\bullet-}$. Milliseconds after formation and isolation of the radical anion $SiO_3^{\bullet-}$ in a 1×10^{-6} Torr H_2S atmosphere, the spectrum consisted primarily of *m*/*z* 76 ($SiO_3^{\bullet-}$) and a lower abundance ion at *m*/*z* 77 (SiO_3H^-). Ab initio structures for $SiO_3^{\bullet-}$ and SiO_3H^- were generated for comparison with the S-bearing species and are presented in Figure 3. At longer reaction times, the abundance of SiO_3H^- increased, followed sequentially by two other product ions at *m*/*z* 93 and *m*/*z* 109. As in the case of the reaction of H_2S with $SiO_2^{\bullet-}$, these latter two ions correspond to SiO_2SH^- and $SiOS_2H^-$. A kinetic plot of the abundances of these ions indicated that they are related by three sequential reactions (Figure 4). In forming SiO_3H^-, $SiO_3^{\bullet-}$ abstracts the radical H$^\bullet$ from H_2S (reaction 3). Once

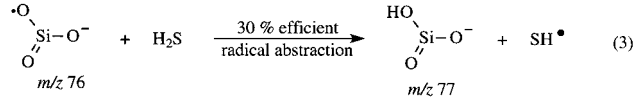

formed, SiO_3H^- reacts with a second H_2S molecule by exchanging O-for-S, forming SiO_2SH^- and eliminating H_2O in the process (reaction 4). SiO_2SH^- then reacts with a third H_2S, exchanging O-for-S to form $SiOS_2H^-$ and eliminating H_2O (reaction 2 again). As noted previously, a third O-for-S exchange does not occur.

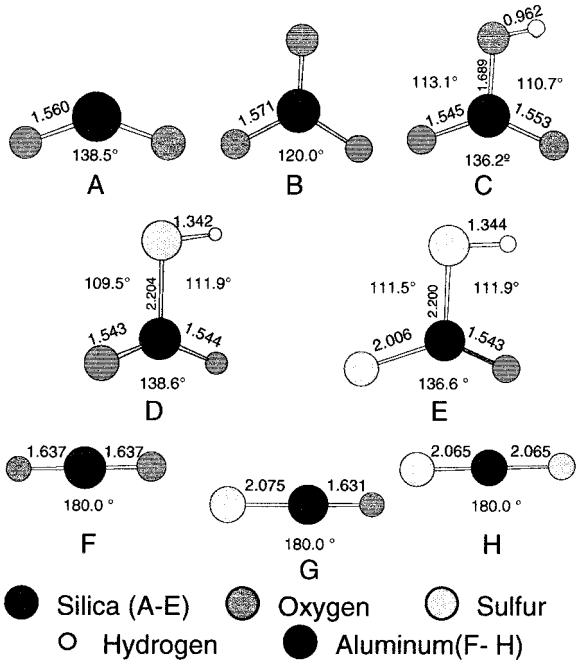

Figure 3. Ab initio structures determined by B3LYP/6-311+G(2d,2p) of (A) $SiO_2^{\bullet-}$, (B) $SiO_3^{\bullet-}$, (C) SiO_3H^-, (D) SiO_2SH^-, (E) $SiOS_2H^-$, (F) AlO_2^-, (G) $AlOS^-$, and (H) AlS_2 bond lengths are listed in Å and bond angles in degrees.

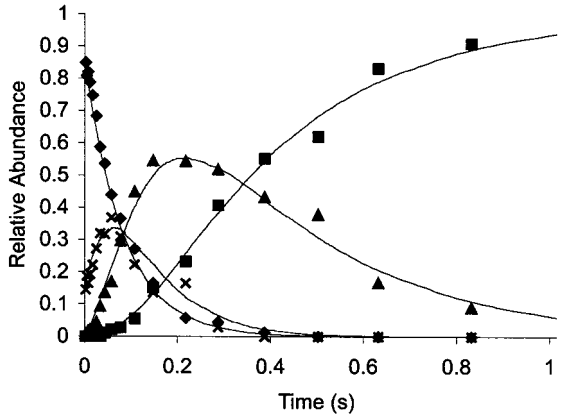

Figure 4. Kinetic plot, and stochastic kinetic model of the consecutive reactions $SiO_3^{\bullet-} \rightarrow SiO_3H^-$, $SiO_3H^- \rightarrow SiO_2SH^-$, and $SiO_2SH^- \rightarrow SiOS_2H^-$, where $k_1 = 3.5 \times 10^{-10}$, $k_2 = 4.5 \times 10^{-10}$, and $k_3 = 1.0 \times 10^{-10}$ cm^3 molecule^{-1} s^{-1}. $SiO_3^{\bullet-}$ data (◆), SiO_3H^- data (×), SiO_2SH^- data (▲), $SiOS_2H^-$ data (■). Lines represent stochastic kinetic model. $P(H_2S) = 1.0 \times 10^{-6}$ Torr.

The rate constant for the disappearance of $SiO_3^{\bullet-}$ was calculated from the semilog plot of *m*/*z* 76 versus time and resulted in a value of 3×10^{10} cm^3 molecule^{-1} s^{-1}, which is about 30% of the ADO collision constant. The rate constant for the reaction of $SiO_3H^- + H_2S \rightarrow SiO_2SH^- + H_2O$ was estimated at 5×10^{-10} cm^3 molecule^{-1} s^{-1}, (40% of the ADO constant) using stochastic kinetic modeling. The rate constant for the third reaction $SiO_2SH^- + H_2S \rightarrow SiOS_2H^- + H_2O$ was estimated at 1.0×10^{-10} cm^3 molecule^{-1} s^{-1} using the stochastic model, which corresponds to an efficiency of 8%. This value was in good agreement with that estimated for the same reaction starting from $SiO_2^{\bullet-}$ (above).

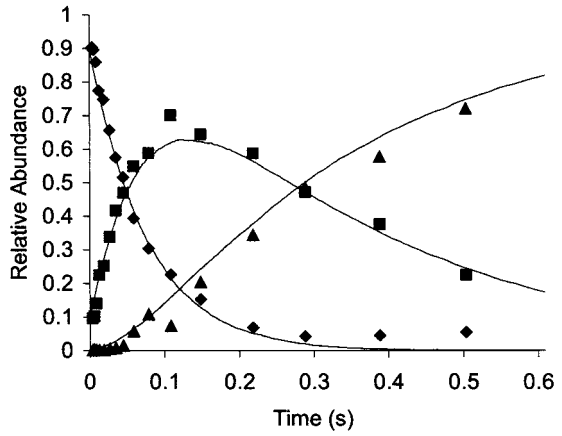

Figure 5. Kinetic plot and stochastic kinetic model for the consecutive reactions $SiO_3H^- \rightarrow SiO_2SH^-$, and $SiO_2SH^- \rightarrow SiOS_2H^-$. SiO_3H^- data (◆), SiO_2SH^- data (■), $SiOS_2H^-$ data (▲). Lines represent stochastic kinetic model. $P(H_2S) = 1.1 \times 10^{-6}$ Torr.

SiO_3H^-. When even-electron SiO_3H^- (*m*/*z* 77) was formed and isolated in the H_2S atmosphere, it underwent two consecutive O-for-S exchange reactions to form SiO_2SH^- (*m*/*z* 93) and $SiOS_2H^-$ (*m*/*z* 109). The kinetic plot for the three ions clearly indicated the sequential nature of the two O-for-S exchange reactions (Figure 5). The rate constant for the conversion of SiO_3H^- to SiO_2SH^- (reaction 4) was measured directly at 4×10^{-10} cm^3 molecule^{-1} s^{-1}, which implies that the reaction is approximately 30% efficient. This value is less than that estimated for SiO_3H^- formed from $SiO_3^{\bullet-} + H_2S$ using stochastic kinetic modeling (40%) starting from $SiO_3^{\bullet-}$, but we consider the agreement to be reasonable given the uncertainty of the rate constant measurements. The rate constant for the conversion of SiO_2SH^- to $SiOS_2H^-$ was estimated at 0.9×10^{-10} cm^3 molecule^{-1} s^{-1} using stochastic kinetic modeling, which is equivalent to 8% efficiency, identical to the efficiency estimated for SiO_2SH^- formed from $SiO_2^{\bullet-}$ and $SiO_3^{\bullet-}$.

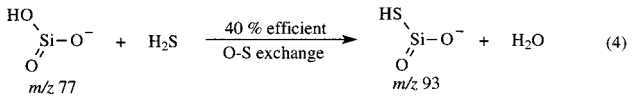

AlO_2^-. The even-electron anion AlO_2- (*m*/*z* 59) was also observed to react efficiently with H_2S. Reaction products appeared at *m*/*z* 75 and 91 that corresponded to $AlOS^-$ and AlS_2^-, respectively. Ion assignments were substantiated by the appearance of ^{34}S isotopic ions at *m*/*z* 77 and 93, and by experiments using D_2S, in which the product ion masses did not shift. Product ions having these compositions would arise from consecutive O-for-S exchange reactions (reactions 5 and 6),

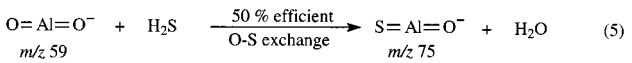

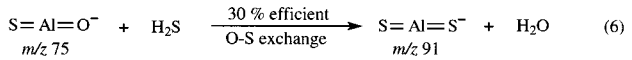

consistent with the appearance of the kinetic plot (Figure 6). The semilog plot of AlO_2^- abundance versus time resulted in a measured rate constant of 6×10^{-10} cm^3 molecule^{-1} s^{-1} for reaction 5, which corresponds to 50% efficiency. Stochastic kinetic modeling resulted in an estimated rate constant for $AlOS^- + H_2S \rightarrow AlS_2^- + H_2O$ of 4×10^{-10} cm^3 molecule^{-1} s^{-1}, that corresponds to 30% efficiency.

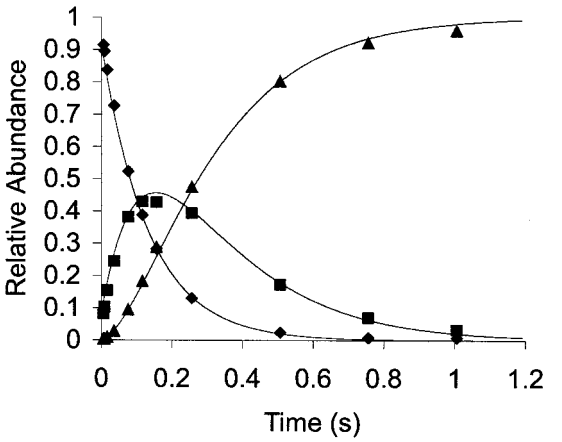

Figure 6. Kinetic plot and stochastic kinetic model for the consecutive reactions $AlO_2^- \rightarrow AlOS^-$, and $AlOS^- \rightarrow AlS_2^-$. AlO_2^- data (◆), $AlOS^-$ data (■), AlS_2^- data (▲). Lines represent stochastic kinetic model. $P(H_2S) = 4.0 \times 10^{-7}$ Torr.

The reactivity of AlO_2^- with H_2S was more than 10 times faster than reaction with water,[15] which may reflect the fact that H_2S is 39 kcal mol^{-1} more acidic than H_2O.[41] In addition, the reaction pathway is significantly different. When AlO_2^- reacts with H_2O, two sequential addition steps occur, eventually forming tetracoordinate $AlO_4H_4^-$.[15] In contrast, when reacting with H_2S, Al does not even trigonally coordinate but instead maintains a bicoordinate structure by eliminating H_2O. The ab initio calculations indicated that the structures of AlO_2^-, $AlOS^-$, and AlS_2^- were linear (Figure 3).

IV. Summary

Odd-electron anions $SiO_2^{\bullet-}$ and $SiO_3^{\bullet-}$ react with H_2S by efficient radical abstraction to produce even electron product ions SiO_2SH^- and SiO_3H^-, respectively. $SiO_2^{\bullet-}$ could be considered undercoordinated; therefore, it readily abstracts a $^{\bullet}SH$ radical. $SiO_3^{\bullet-}$ is coordinated to the extent that it will not abstract a $^{\bullet}SH$ but instead abstracts an $^{\bullet}H$. In contrast, the even-electron anions SiO_3H^- and AlO_2^- do not abstract radicals from H_2S but rather undergo efficient O-for-S exchange reactions producing even electron SiO_2SH^- and $AlOS^-$, respectively. These reactions are necessarily complex and require the transfer of both H atoms from H_2S to a departing O for the elimination of H_2O. The even electron product ions SiO_2SH^- and $AlOS^-$ undergo a subsequent O-for-S exchange reaction, producing $SiOS_2H^-$ and AlS_2^-.

Future directions are to extend these studies to other mineral oxide materials. For example, preliminary investigations have shown that oligomeric aluminosilicate anions $Al_mSi_nO_{2(m+n)}H_{(m-1)}^-$ [42] will participate in O-for-S exchange reactions but that these reactions are in competition with very fast H_2O condensation reactions that approach unit efficiency. It is possible that O-for-S exchange may occur for hydrated oligomeric anions that would be chemically more similar to the surfaces of mineral dust or colloidal particles than would the monomeric anions.

The results presented in this paper, along with preliminary results for the $Al_mSi_nO_{2(m+n)}H_{(m-1)}^-$ systems mentioned above, may represent mechanisms by which sulfur is incorporated into silicate or aluminate minerals, which would have the potential for impacting geochemical or atmospheric sulfur budgets. The reactions do not support the oxidation of H_2S in contact with aluminate-, or silicate-oxyanion moieties, at least under the conditions of the H_2S atmosphere present in the IT-SIMS. In contrast, reduced sulfide species are formed, and thus the

O-for-S exchange reactions instead may be relevant to the formation of metal sulfides from oxides under reducing conditions. Extension of the studies to transition metal oxides would enable the evaluation of this hypothesis.

Acknowledgment. The authors thank Jim Delmore, Dave Dahl, and John Olson for insightful discussion and assistance with instrument design and modification. This research was supported by the United States Department of Energy, under contract DE-AC07-99ID13727 BBWI.

Supporting Information Available: Figure 1S contains spectra for the three sequential reactions $SiO_3^- + H_2S \rightarrow SiO_3H^- + {}^{\bullet}SH$, $SiO_3H^- + H_2S \rightarrow SiO_2SH^- + H_2O$, and $SiO_2SH^- + H_2S \rightarrow SiOS_2H^- + H_2O$. Figure 2S contains spectra for the two sequential reactions $SiO_3H^- + H_2S \rightarrow SiO_2SH^- + H_2O$, and $SiO_2SH^- + H_2S \rightarrow SiOS_2H^- + H_2O$. Figure 3S contains spectra for the reaction $AlO_2^- + H_2S \rightarrow AlOS^- + H_2O$, and $AlOS^- + H_2S \rightarrow AlS_2^- + H_2O$. This material is available free of charge via the Internet at http://pubs.acs.org.

References and Notes

(1) Jeong, C.-H.; Kim, C.-S.; Kim, S.-J.; Park, S.-W. *J. Environ. Sci. Health* **1996**, *A31*, 2173−2192.

(2) Groenewold, G. S.; Ingram, J. C.; McLing, T.; Gianotto, A. K.; Avci, R. *Anal. Chem.* **1998**, *70*, 534−539.

(3) Turner, G. D.; Zachara, J. M.; McKinley, J. P.; Smith, S. C. *Geochim. Cosmochim. Acta* **1996**, *60*, 3399−3414.

(4) Buseck, P. R.; Posfai, M. *Proc. Nat. Acad. Sci. U.S.A.* **1999**, *96*, 3372−3379.

(5) Song, C. H.; Carmichael, G. R. *Atmos. Environ.* **1999**, *33*, 2203−2218.

(6) Zhou, G.; Tazaki, K. *Atmos. Environ.* **1996**, *30*, 3301−3308.

(7) Sposito, G. S.; Skipper, N. T.; Sutton, R.; Park, S.-H.; Soper, A. K.; Greathouse, J. A. *Proc. Nat. Acad. Sci. U.S.A.* **1999**, *96*, 3358−3364.

(8) Brookins, D. G.; Thomson, B. M.; Longmire, P. A.; Eller, P. G. *Radioact. Waste Manage. Environ. Restor.* **1993**, *17*, 269−287.

(9) Garcia, C. L.; Lercher, J. A. *J. Phys. Chem.* **1992**, *96*, 2230−2235.

(10) Laperdrix, E.; Sahibed-dine, A.; Costentin, G.; Saur, O.; Bensitel, M.; Nedez, C.; Saad, A. B. M.; Lavalley, J. C. *Appl. Catalysis B, Environ.* **2000**, *26*, 71−80.

(11) Feuerriegel, U.; Klose, W.; Sloboshanin, S.; Goebel, H.; Schaefer, J. A. *Langmuir* **1994**, *10*, 3567−3570.

(12) Hoyos, L. J.; Primet, M.; Praliaud, H. *J. Chem. Soc., Faraday Trans.* **1992**, *88*, 113−119.

(13) Portela, L.; Grange, P.; Delmon, B.; Topsoe, H.; Knozinger, H.; Conner, W. C. *Stud. Surf. Sci. Catal.* **1993**, *75*, 559−569.

(14) Groenewold, G. S.; Appelhans, A. D.; Gresham, G. L.; Olson, J. E.; Jeffery, M.; Wright, J. B. *Anal. Chem.* **1999**, *71*, 2318−2323.

(15) Scott, J. R.; Groenewold, G. S.; Gianotto, A. K.; Benson, M. T.; Wright, J. B. *J. Phys. Chem. A* **2000**, *104*, 7079−7090.

(16) Groenewold, G. S.; Scott, J. R.; Gianotto, A. K.; Hodges, B. D. M.; Kessinger, G. F.; Wright, J. B., unpublished results, 2001.

(17) Freitas, M. A.; Shi, S. D. H.; Hendrickson, C. L.; Marshall, A. G. *J. Am. Chem. Soc.* **1998**, *120*, 10187−10193.

(18) Groenewold, G. S.; Appelhans, A. D.; Ingram, J. C. *J. Am. Soc. Mass Spectrom.* **1998**, *9*, 35−41.

(19) Groenewold, G. S.; Appelhans, A. D.; Ingram, J. C.; Gresham, G. L.; Gianotto, A. K. *Talanta* **1998**, *47*, 981−986.

(20) Ingram, J. C.; Appelhans, A. D.; Groenewold, G. S. *Int. J. Mass Spectrom. Ion Proc.* **1998**, *175*, 253−262.

(21) Delmore, J. E.; Appelhans, A. D.; Peterson, E. S. *Int. J. Mass Spectrom. Ion Proc.* **1995**, *146/147*, 15−20.

(22) Appelhans, A. D.; Delmore, J. E. *Anal. Chem.* **1989**, *61*, 1087−1093.

(23) Groenewold, G. S.; Delmore, J. E.; Olson, J. E.; Appelhans, A. D.; Ingram, J. C.; Dahl, D. A. *Int. J. Mass Spectrom. Ion Proc.* **1997**, *163*, 185−195.

(24) Bartmess, J. E.; Georgiadis, R. M. *Vacuum* **1983**, *33*, 149−153.

(25) *Practical Aspects of Ion Trap Mass Spectrometry*; Todd, J. F. J., Ed.; CRC Press: New York, 1995; Vol. 1, p 4.

(26) Frisch, M. J.; Trucks, G. W.; Schlegel, H. B. S., G. E.; Robb, M. A.; Cheeseman, J. R.; Zakrzewski, V. G.; Montgomery-Jr., J. A.; Stratmann, R. E.; Burant, J. C.; Dapprich, S.; Millam, J. M.; Daniels, A. D.; Kudin, K. N.; Strain, M. C.; Farkas, O.; Tomasi, J.; Barone, V.; Cossi, M.; Cammi, R.; Mennucci, B.; Pomelli, C.; Adamo, C.; Clifford, S.; Ochterski, J.; Petersson, G. A.; Ayala, P. Y.; Cui, Q.; Morokuma, K.; Malick, D. K.; Rabuck, A. D.; Raghavachari, K.; Foresman, J. B.; Cioslowski, J.; Ortiz, J. V.; Stefanov, B. B.; Liu, G.; Liashenko, A.; Piskorz, P.; Komaromi, I.; Gomperts, R.; Martin, R. L.; Fox, D. J.; Keith, T.; Al-Laham, M. A.; Peng, C. Y.; Nanayakkara, A.; Gonzalez, C.; Challacombe, M.; Gill, P. M. W.; Johnson, B.; Chen, W.; Wong, M. W.; Andres, J. L.; Gonzalez, C.; Head-Gordon, M.; Replogle, E. S.; Pople, J. A. Gaussion 98; Revision A.4 ed.; Gaussian, Inc.: Pittsburgh, PA, 1998.

(27) Becke, A. D. *J. Chem. Phys.* **1993**, *98*, 5648.

(28) Lee, C.; Yang, W.; Parr, R. *Phys. Rev. B* **1988**, *37*, 785.

(29) Peng, C. J. *Israel J. Chem.* **1994**, *33*, 449.

(30) Peng, C. J. *Comput. Chem.* **1996**, *17*, 49.

(31) Chesnavich, W. J.; Su, T.; Bowers, M. T. *J. Chem. Phys.* **1980**, *72*, 2641−2655.

(32) Su, T.; Bowers, M. T. *Int. J. Mass Spectrom. Ion Phys.* **1973**, *12*, 347−356.

(33) Su, T.; Bowers, M. T. *Int. J. Mass Spectrom. Ion Phys.* **1975**, *17*, 211−212.

(34) Goeringer, D. E.; McLuckey, S. A. *Int. J. Mass Spectrom. Ion Proc.* **1998**, *177*, 163−174.

(35) Gronert, S. *J. Am. Soc. Mass Spectrom.* **1998**, *9*, 845−848.

(36) Gillespie, D. T. *J. Phys. Chem.* **1977**, *81*, 2340−2361.

(37) Hinsberg, W. D.; Houle, F. A. Chemical Kinetics Simulator v.1.01. The program package, including supporting documentation, is available for a no-cost license from IBM at http://www.almaden.ibm.com/st/msim/. A reference for the basic algorithm is D. J. Gillespie, *J. Comput. Phys.* **1976**, *22*, 403. 1.01 ed.; http://www.almaden.ibm.com/st/msim/, 2000; Vol. 2000.

(38) Benson, S. W. *The Foundation of Chemical Kinetics*; McGraw-Hill: New York, 1960.

(39) Moore, J. W.; Pearson, R. G. *Kinetics and Mechanism*, 3rd ed.; John Wiley: New York, 1981.

(40) Vickerman, J. C.; Briggs, D.; Henderson, A. The Static SIMS Library; Surface Spectra Ltd.: Manchester, UK, 1999.

(41) Lias, S. G.; Bartmess, J. E.; Liebman, J. F.; Holmes, J. L.; Levin, R. D.; Mallard, W. G. Ion Energetics Data. In *NIST Chemistry WebBook, NIST Standard Reference Database Number 69, February 2000*; Mallard, W. G., Linstrom, P. J., Eds.; National Institute of Standards and Technology (http://webbook.nist.gov): Gaithersburg MD, 20899, 2000.

(42) Groenewold, G. S.; Kessinger, G. F.; Scott, J. R.; Gianotto, A. K.; Appelhans, A. D.; Delmore, J. E. *Anal. Chem.* **2001**, *73*, 226−232.